AWESW2022
21st Australasian Wind Engineering Society Workshop
2 – 3 February, 2023

Wind Tunnel Testing of Torsional Instability in Single-Axis Solar Trackers: Summary of Methodologies and Results

Parsa Enshaei[1], Jubayer Chowdhury[2], Heather Sauder[3], David Banks[4]
[1]CPP Wind Engineering, St. Peters, 2044, NSW, Australia, penshaei@cppwind.com
[2]CPP Wind Engineering, Windsor, 80550, Colorado, United States, jchowdhury@cppwind.com
[3]CPP Wind Engineering, Windsor, 80550, Colorado, United States, hsauder@cppwind.com
[4]CPP Wind Engineering, Windsor, 80550, Colorado, United States, dbanks@cppwind.com

ABSTRACT

Single-axis tracker (SAT) failures have been frequently observed at wind speeds lower than the site design wind speed. Over the past decade, torsional instability has been highlighted as the cause for most of these failures. A review of the instability mechanisms and the limitations associated with section model testing for quantifying the wind speeds causing torsional instability are discussed. The design, construction, and testing methods recommended for SAT aeroelastic instability testing are presented, followed by resulting generalized instability curves based on dozens of tested configurations. The critical wind speed trend with tilt is a W-shaped curve for low damping levels, below 10%-of-critical, while additional damping is seen to flatten the curve, before transitioning to a U-shaped curve as damping is further increased. New challenges with evolving SAT designs and corresponding adaptation of testing requirements are also highlighted.

1. Background

The solar industry is fast-growing and cost-competitive, with frequent changes in products, including the mounting structures. Single-axis trackers (SATs) are popular due to their increased power generation compared to their fixed-tilt counterparts. The conventional SAT consists of panels mounted onto a north-south orientated central torque tube, with multiple bearing posts along the span. One or more drives provide torque to drive and optimize the power generated from the panels tracking the sun. A schematic of the key components in a conventional SAT is shown in Figure 1.

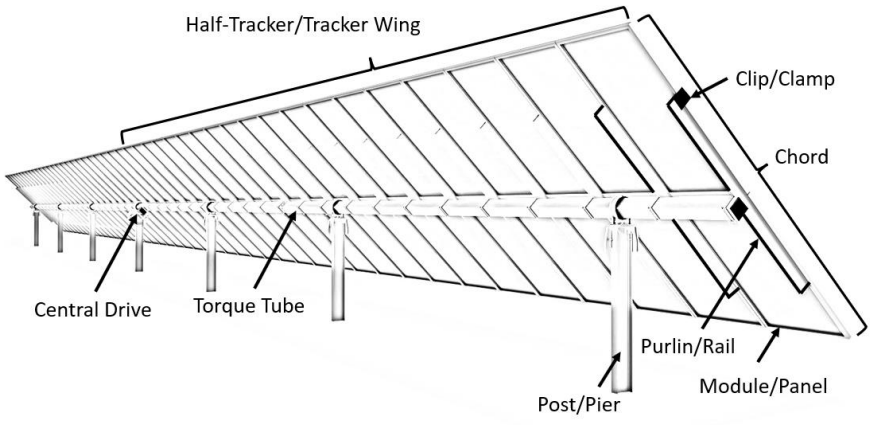

Figure 1. Conventional single-drive SAT schematic with typical components outlined

Weather events account for a significant number of insurance claims for SATs, with aeroelastic torsional instability highlighted as the cause for several failures, one of which has been investigated by Valentin *et al.* (2022). Furthermore, torsional instability in SATs has been the subject of limited publications over the past decade; Rohr *et al.* (2015), Young *et al.* (2020), and Martinez-Garcia *et al.* (2021). The instability phenomenon is attributed to various mechanisms such as torsional galloping, single-degree of freedom flutter (SDOF), and torsional divergence.

Most SATs have a policy of rotating into a stow position (pre-determined tilt) during high wind events. To determine a suitable stow tilt, SAT designers consider the trade-off between the wind loads across all components and the potential for aeroelastic instability. As an input to this decision process, the variation of the critical wind speed, U_{cr}, at which instability is observed across all tilts is required. This is sometimes referred to as the "instability curve" or "U_{cr} curve".

1.1 Torsional instability mechanisms

The Rohr *et al.* (2015) section model CFD study of torsional instability of SATs described the low-tilt instability mechanisms, schematically shown in Figure 2a. At the time, it was referred to as torsional galloping, but we now believe it is better described as cyclical torsional divergence. A vortex forms at the top (or bottom) side of the leading edge, pulling the leading edge up (or down). This instability occurs when the tracker is stowed flat or near flat (i.e. close to 0°). As the tracker tilts further from flat, the torsional resistance from the twisting torque tube increases linearly. However, the torque due to the suction region beneath the vortex at the leading edge increases at the same or faster rate than this resistance. The resulting motion is slower than the torsional natural frequency of the tracker, at least when the tracker is being pulled away from flat. At a high enough tilt (much higher than would be predicted by a quasi-steady divergence model), the vortex is released, and the tracker springs past the initial (near flat) position. If the tracker travels significantly past 0°, then a new leading-edge vortex is formed on the opposite side to the previous cycle, and the process continues and amplitude increases. This stiffness-driven mechanism is not sensitive to moderate levels of damping and is purely a function of the trade-off between wind-induced torque and the torsional stiffness of the torque tube. The mechanism and its characteristics are described in further detail in an upcoming study, Enshaei *et al.* (2023).

A second instability mechanism is evident at modest tilts from 10° to 45°. This instability can be controlled with damping. Based on 2D CFD simulations, we believe it is best described as vortex lock-in, because it is characterized by conventional Von Karman vortex-street shedding from alternating edges of the leeward side, Figure 2b. If the tracker motion grows significantly and crosses the 0° tilt, it may transition to cyclical torsional divergence. Conversely, this motion can be initiated by a torsional divergence oscillation cycle which is not large enough to cause the tracker to return past 0°.

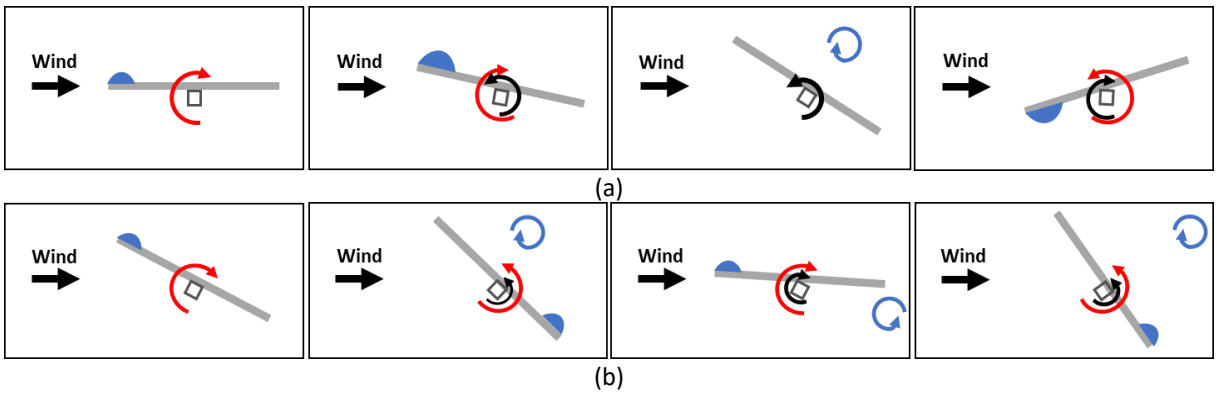

Figure 2. Schematics of the torsional instability mechanisms observed; (a) cyclical torsional divergence, (b) vortex lock-in. Flow structures (separation bubble and shed vortices) are shown in blue, the resulting wind load torque is shown in red, and the structures spring force in black.

1.2 Section model testing

Section model testing has been used to study fluid structure interaction of SATs with wind tunnel, Quintela *et al.* (2020), and numerical simulations; Rohr *et al*. (2015) and Young *et al.* (2020). In most cases, a section model test uses a geometrically and structurally representative section of an isolated tracker, as is typically done for bridges.

Multi-row aeroelastic SAT testing on a turntable has shown that there are limitations and challenges with using section models to assess aeroelastic instability across a tracker array.

- At some tilts, far interior rows can experience instability at wind speeds lower than an isolated perimeter row especially during cornering winds. Section models cannot model cornering winds.
- The aeroelastic deflection and motion of upwind and downwind rows impact the flow environment for surrounding trackers and needs to be modelled because:
    - Vortex shedding from the upstream trackers can trigger instability in the downstream rows.
    - Deflected perimeter rows can provide sheltering and delay interior row instability in some cases.
    - A typical tracker array will include stiffer trackers in the perimeter than the interior rows. The interior tracker flow environment will therefore change with the dynamic response of the perimeter trackers.
    - It is not clear if the wake generated by a uniformly twisting section model matches the wake generated by the helical deflected shape of a 3D tracker.

Regardless of the number of rows modelled, assumptions are required to adapt section model testing to predict three-dimensional fluid-structure effects. The moving tracker has a helical twisted shape, with little or no motion near the drive post. We refer to the proportion of the tracker that is moving enough to be actively affected by the instability mechanisms described above as 'participation fraction'. Our work shows that the participation fraction varies across designs and can only be correctly captured through a full aeroelastic model.

Unlike bridges, SATs are very close to the ground, and are immersed in a turbulence flow field with a significant vertical velocity gradient. Many section model tests are conducted in smooth flow, such as Quintela *et al.* (2020). Our work indicates that this is not conservative. In addition, the sudden nature of cyclical torsional divergence requires the mean speed in a smooth flow test to be considered as a gust speed.

2. Aeroelastic Wind Tunnel Testing

The full aeroelastic models of SATs used in this paper have been constructed at geometric scales ranging from 1:20 to 1:35. The results are from 36 test configurations across 16 different designs. To achieve dynamic similarity between the model and full-scale prototype, the critical parameter is the torsional stiffness of the torque tube, which is a function of the torsional rigidity of the tube and the flexible span length. This controls the deflection of the structure under wind loads, and the consequent changes in the fluid-structure interaction. This is particularly important at low tilts, where it determines the stiffness-driven cyclical torsional divergence. The mass moment of inertia and damping are also modelled to match the torsional natural frequency and damping level. Using dimensional analysis, the required structural parameters can be scaled by the following equations, as stated in ASCE 49-21 (2021):

$$\frac{(GJ)_m}{\rho_m U_m^2 L_m^4} = \frac{(GJ)_p}{\rho_p U_p^2 L_p^4} \tag{1}$$

$$\frac{I_m}{\rho_m L_m^5} = \frac{I_p}{\rho_p L_p^5} \tag{2}$$

$$\zeta_m = \zeta_p \tag{3}$$

where

GJ = Torsional rigidity of the torque tube; G is the shear modulus and J is the torsional constant
ρ = Air density
U = Wind velocity
L = Reference length; typically taken as the chord length for SATs
I = Mass moment of inertia
ζ = Damping ratio
m, p = Model and prototype (full-scale)

Aeroelastic models and test setup for a tracker design are shown in Figure 3. In most tests, six or more rows of trackers were tested in a generic rectangular configuration. The velocity scale was determined based on the torsional stiffness, which was modelled using spring steel rods of different diameters, depending on the overall torsional rigidity of the full-scale tracker sections. For single-drive SATs, the flexible section was taken as one half-tracker span (assuming symmetry), whilst for multi-drive systems, the longest fixed-free span (cantilever to outer drive post) and fixed-fixed span (two adjacent drive posts) were modelled. When required, additional non-aeroelastic sections were included to aerodynamically model the adjacent tracker sections or rows. Rigid posts with bearings are spaced along the span to support the tracker deck, with a rotationally fixed post at the driving post locations. The steel rod is significantly smaller than the geometrically scaled torque tube, and additional material such as hollow 3D printed pieces or foam were used to aerodynamically model the torque tube and maintain the correct pressure distribution underneath the panels, as discussed by Chowdhury *et al.* (2022). Mass moment of inertia was modelled using different types of wood based on mass, and in some cases carbon fiber for heavier panels. Damping ratio was matched to measurements from full-scale prototypes, through inherent damping of the scaled models or addition of supplementary friction dampers. Free decay tests were conducted on the models to confirm torsional natural frequencies and damping levels were correctly modelled.

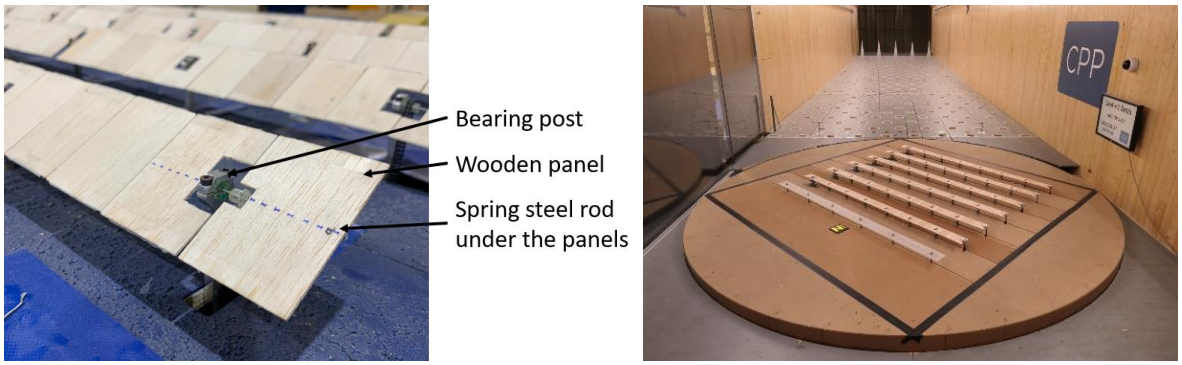

Figure 3. Close-up of a generic SAT aeroelastic model (left) and multi-row SAT models in the wind tunnel (right)

Most configurations were tested in an open country approach profile, Exposure C in ASCE 49-21 (2021). Limited testing was conducted in a more turbulent suburban approach, Exposure B, which typically decreased U_{cr}. Angular displacements of the modelled tracker sections were measured using lasers or potentiometers where maximum rotation was observed. The wind speed was gradually increased until one or more of the trackers experienced significant motion, at which point the wind speed was gradually decreased. There was some evidence of hysteresis, where trackers remained unstable below the speed at which instability was initially triggered. Wind speeds were measured by an upstream pitot-static system or hot film, with a frequency response that was able to capture gust speeds. Given the scale of the models, a partial turbulence method was used ASCE 49-21 (2021). Wind directions varied from +30° to -30°, where 0° is normal to the tracker axis. The positive wind directions are cornering winds over the exposed ends of the tracker. The aeroelastic models were tested for a wide range of tilts, with this paper focusing on tilts within ±45°. Positive tilt refers to leading edge up.

3. Results and Discussion

The critical wind speed, U_{cr}, is noted when a peak-to-peak angular motion greater than 30° is recorded for at least one of the tracker rows. This is significantly larger than buffeting effects due to fluctuations in wind speed, and typically enough to damage SATs. The variations of critical wind speed with tilt is shown in Figure 4. The three subplots in Figure 4 are categorized by damping levels, with results of at least ten test configurations included in each subplot. The shaded grey area envelopes the maximum and minimum values at each tilt from instability curves of the tested configurations. The instability curve from each test is normalized by U_{cr} at 0° tilt, which is not affected by damping up to the levels considered, 30%-of-critical. The normalized values at each tilt and damping level are then averaged, and a smoothed line (solid black) is drawn to show the generalized instability curve with changes in damping. Other than damping, the variation between the results from different test configurations, indicated by the shaded grey area, are a function of several parameters such as chord length, torsional stiffness, inertia, height, row spacing, natural frequency, and perimeter/interior stiffness ratio. Regardless, the plotted generalized instability curves provide an accurate qualitative visualization of the U_{cr} trend with tilt.

At low damping levels (below 10%-of-critical, typical of systems with low friction), the resulting instability curves are W-shaped, centered about 0° to -5°. A significant drop in critical wind speed from 0° is observed at moderate tilts of ±10° and ±20°, with a lower and wider U_{cr} trough and slower high-tilt recovery for the positive tilts than negative tilts. The W-shape of the curve is in good agreement with the Stability Diagram presented by Martinez-Garcia *et al.* (2021), with a damping ratio of less than 1% for their tested models. However, the lower positive tilt U_{cr} relative to negative tilts is due to including internal rows in the current study, which determined the minimum U_{cr} across the array at positive tilts.

As a result of modest supplementary damping or variations in design, such as more bearing posts or additional friction in the bearing housing assembly, the damping ratio can increase to a range of 10-20% (with a caveat that friction is not well-represented by a fraction of critical viscous damping). At this damping level, a flatter W-shaped curve is observed, with less reduction in U_{cr} from 0° to moderate tilts. A similar improvement in stability is noted for the higher tilts, with marginally lower values at the positive tilts compared to negative. Further increasing the damping levels to 20-30% (which typically requires supplementary damping), the instability curve transitions to a V- or U-shaped curve. Relative to U_{cr} at 0°, the critical wind speeds at moderate and high tilts are significantly improved. Across all tilts, U_{cr} can be improved by increasing torsional stiffness through shortening the span or increasing torsional rigidity. At moderate to high tilts, damping can significantly improve the critical wind speed.

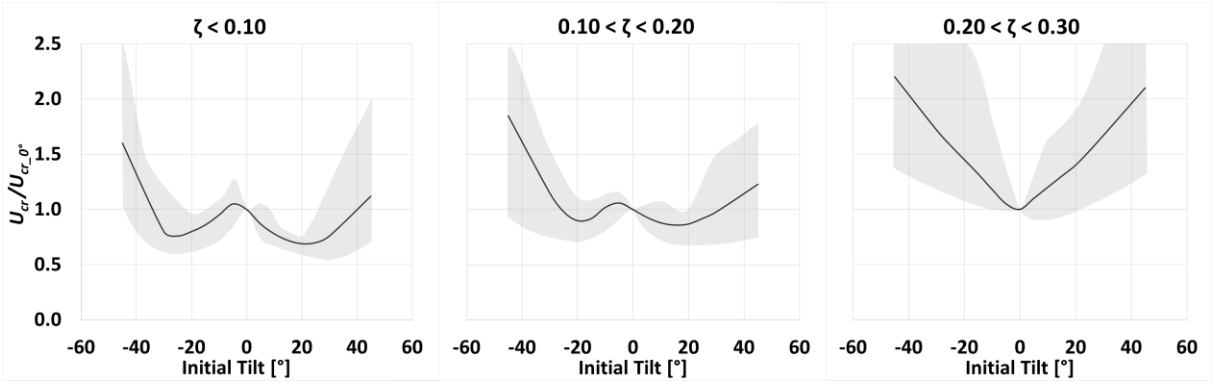

Figure 4. Trend of critical wind speed with initial tilt for the tested SAT designs and configurations, grouped by damping level. Shaded area envelopes values from all configurations. Solid black line is the smoothed average.

4. Conclusions and New Challenges

Multi-row aeroelastic testing in an atmospheric boundary layer approach flow has been performed for dozens of single axis trackers to characterize the changes in critical wind speed with tilt. Grouping the resulting instability curves by damping levels yields a clear set of trends for U_{cr} changes with tilt. W-shaped curves are observed for low damping levels, while additional damping is seen to flatten the curve, before transitioning to a U-shaped curve as damping is further increased.

SAT designs continue to change to reduce the potential for torsional instability. In designs where a low tilt (±3°) stow position is preferred, multiple drives along the tracker span are added to act as rotationally fixed points. This leads to higher torsional stiffness, and the resulting torsional frequencies are relatively high (2-3 Hz). If the posts are not strengthened, the first torsional modes may now include strong-axis post bending. In such cases, three-dimensional aeroelastic modelling to include flexible posts is required. Similarly, if a SAT has flexibility in the drive connection, this must also be modelled.

For designs with a high tilt stow (typical for systems with a single central drive), supplementary damping is often required. Whether the additional damping is from a viscous damper or friction damping at the post top bearings, the additional damping will affect the dynamic behavior of the structure, with the potential for significant changes in the torsional mode shapes. For example, if the damping is high enough, the span between the damper and the drive motor can go unstable. It is important to match not only the damping levels in the wind tunnel, but also the nature of the damping. For instance, distributed friction damping should be modelled with distributed friction dampers. Designers also need to consider the potential for reductions in damping over time, as friction surfaces wear smooth or supplementary viscous dampers leak. To match the required changes in aeroelastic models, the testing methodologies and acquisition techniques would require updates and are considered as part of the ongoing research.

References

American Society of Civil Engineers (ASCE), (2021), "Wind tunnel testing for buildings and other structures", ASCE/SEI 49-21.

Chowdhury J., Sauder H., Banks D., (2022), Effect of solar panel support structure on the wind loading of horizontal single-axis trackers, *Proceedings of the 14th Americas Conference on Wind Engineering,* Lubbock, Texas, May 17-19.

Enshaei P., Chowdhury J., Sauder H., Banks D., (2023), Low-tilt torsional instability of single-axis trackers, Submitted for *16th International Conference on Wind Engineering*, Florence, Italy, August 27-31.

Martinez-Garcia E., Blanco-Marigorta E., Gayo, J.P., Navarro-Manso A., (2021), Influence of inertia and aspect ratio on the torsional galloping of single-axis solar trackers. *Engineering Structures.* 243:112682.

Quintela J., Jurado J.A., Rapela C., Alvarez A.J., Roca M., Hernandez S., Cid Montoya M., Lopez J.M., Ruiz A.J., Moreno I., Jimenez S., (2020), Experimental and computational studies on the performance of solar trackers under vortex shedding, torsional divergence, and flutter. *International Journal of Computational Methods and Experimental Measurements*. 8(4):387-404.

Rohr C., Bourke P.A., Banks D., (2015), Torsional instability of single-axis solar tracking systems, *Proceedings of the 14th International Conference on Wind Engineering,* Porto Alegre – Brazil, June 21-26, 2015, 21-26.

Young E., He X., King R., Corbus D., (2020), A fluid-structure interaction solver for Investigating torsional galloping in solar-tracking photovoltaic panel arrays. *Journal of Renewable and Sustainable Energy*. 12:063503.

Valentin D., Valero C., Egusquiza M., Presas A., (2022), Failure investigation of a solar tracker due to wind-induced torsional galloping. *Engineering Failure Analysis*. 135:106-137